Facile preparation of radium-doped, functionalized nanoparticles as carriers for targeted alpha therapy

Reissig, F.; Hübner, R.; Steinbach, J.; Pietzsch, H.-J.; Mamat, C.;

Originally published:

June 2019

Inorganic Chemistry Frontiers 6(2019), 1341-1349

DOI: https://doi.org/10.1039/c9qi00208a

INORGANIC CHEMISTRY
FRONTIERS

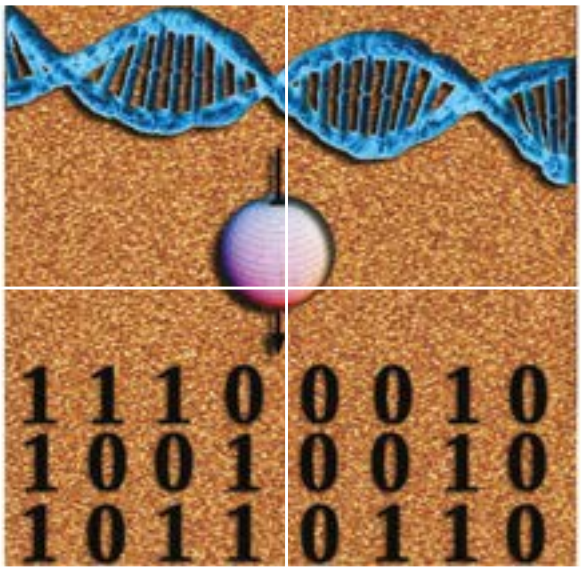

Accepted Manuscript

This article can be cited before page numbers have been issued, to do this please use: F. Reissig, R. Hübner, J. Steinbach, H. Pietzsch and C. Mamat, *Inorg. Chem. Front.*, 2019, DOI: 10.1039/C9QI00208A.

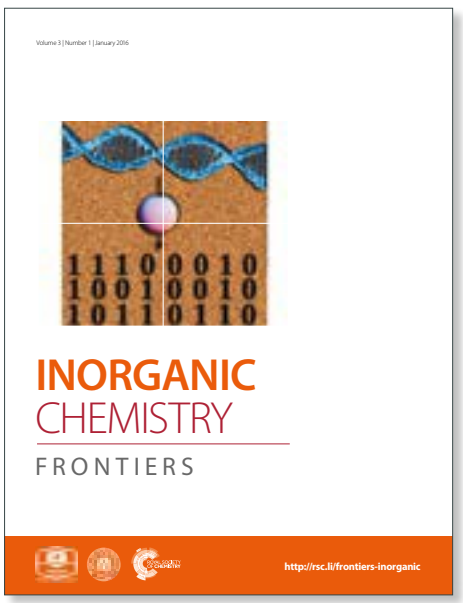

View Article Online
DOI: 10.1039/C9QI00208A

ARTICLE

Facile preparation of radium-doped, functionalized nanoparticles as carriers for targeted alpha therapy

Received 00th January 20xx,
Accepted 00th January 20xx

DOI: 10.1039/x0xx00000x

Falco Reissig,[ab] Rene Hübner,[c] Jörg Steinbach,[ab] Hans-Jürgen Pietzsch [a] and Constantin Mamat *[ab]

Despite its attractive properties, internal targeted alpha particle therapy using $^{223/224}$Ra is currently limited to palliative bone-seeking applications. To make both radioisotopes accessible for the treatment of other cancer diseases, functionalized nanoparticles (NPs) based on $BaSO_4$ are proposed as carriers to stably bind radium to a targeting molecule. Although significant advances in the tailoring of $BaSO_4$-based NPs have been achieved, their preparation is strongly dependent on the use of surfactants and additives. Herein, the direct facile one-pot preparation of radium-doped, alendronate-functionalized $BaSO_4$ NPs from [^{224}Ra]Ra$(NO_3)_2$, $(NH_4)_2SO_4$, $BaCl_2$ and alendronate in an aqueous medium was reported. Remarkably, the size of the formed $BaSO_4$ NPs is independend of the anion used, but is controlled by the addition of organic solvents. Upon the addition of alendronate, amine functionalities were introduced on the NP surface. To evidence this modification, a fluorescence dye-containing alendronate was used. Additionally, a similar fluorescent NBD active ester was applied to proof the reactivity of the outer alendronate amine groups for a later connection of targeting molecules to follow the radiotherapeutic approach. The variations in the functionalities were examined by IR and the morphology of the resulting $BaSO_4$ NPs were investigated in detail. DLS and TEM measurements provided an average diameter of the nanoparticles of approx. 140 nm.

Introduction

Targeted alpha particle therapy (TAT) is continually focused and discussed in radiopharmaceutical research.[1-3] By the connection of alpha-emitting radionuclides with biological targeting units like antibodies, peptides or highly affine small molecules, tumor cells can be affected very efficiently by inducing a high number of double-strand breaks to different tumor tissues such as prostate cancer cells.[4] Due to the high linear energy transfer (LET) of alpha emitters, almost the whole amount of the radionuclide's decay energy will be deposited within four to five cell diameters to effectively destroy the cancer cell and the surrounding healthy tissue will be protected from significant damage.[5-7] Unlike beta-emitters, therapy approaches using alpha irradiation overcome radioresistance of cancer cells.[8]
^{223}Ra and ^{224}Ra are two promising alpha emitters with proper half-lives for TAT. ^{223}Ra in the form of [^{223}Ra]$RaCl_2$ (Xofigo®) is the only EMA- and FDA-approved alpha particles emitting radiopharmaceutical as well as the prime example for the working principle of TAT.[9-11] Based on its calcimimetic behavior, Ra^{2+} is incorporated into the bone structure. Regrettably, the application of [^{223}Ra]$RaCl_2$ is limited to the analgesic, palliative treatment of bone metastases from prostate carcinoma to date.[12,13] To exploit the therapeutic potential of alpha emitters like ^{223}Ra and ^{224}Ra, novel targeting strategies and carrier systems have to be developed. An additional interesting aspect is, that ^{224}Ra and its decay product ^{212}Pb are also seen as an in vivo generator system for the production of the alpha emitter ^{212}Bi,[14,15] even if implications about the recoil effect of the daughter nuclides have to be strongly taken into account.[16,17] Furthermore, working with ^{227}Th as alpha emitting mother nuclide of ^{223}Ra is contemplable.[18]
Until now, a feasible standard complexation method for radium is still not found, even if research regarding calixarene ligands for the complexation of heavy group two metals is in progress.[19-21] Therefore, it is worth to examine alternative carriers like nanoparticles (NPs)[22] or liposomes.[23] For instance, the simple co-precipitation of (Ra)$BaSO_4$ is merely described, but for approaches in environmental chemistry.[24-26] $BaSO_4$ NPs with and without further functionalities have already been focused for different applications, including medical applications like X-ray contrast agents[27] and additives for bone cement.[28] Beyond that, studies have shown that $BaSO_4$ - compared to other nanomaterials - is a less sensitizing material regarding lung absorption and the barium-body-clearance and should be eligible for medical use.[29-31] Although several barium compounds are known to be toxic and the LD_{50} value ($BaCl_2$) for oral exposures on rats was reported as 179 mg/kg body mass, it is not necessary to pursue further purification than centrifugation to remove the free metal ions, since normal preparation methods will use not more than a total of approx. 60 mg of the respective barium salt.[32] $BaSO_4$ itself is described as non-toxic.

[a] Institut für Radiopharmazeutische Krebsforschung, Helmholtz-Zentrum Dresden-Rossendorf, Bautzner Landstraße 400, D-01328 Dresden, Germany.
[b] Fakultät Chemie und Lebensmittelchemie, Technische Universität Dresden, D-01062 Dresden, Germany.
[c] Institut für Ionenstrahlphysik und Materialforschung, Helmholtz-Zentrum Dresden-Rossendorf, Bautzner Landstraße 400, D-01328 Dresden, Germany.

Nanomaterials in general became more and more interesting for targeting approaches in tumor therapy.[33-36] Moreover, it is conceivable, that by the combination of a therapeutic alpha emitting radionuclide like ^{223}Ra on the one hand and the diagnostically applicable barium radioisotope ^{131}Ba (which is in development for cyclotrone production) on the other hand with an almost identical half-life but diagnostic properties,[37-39] individual theragnostic approaches can be pursued. Thus, our present work aims at the development of a simple, clinically transmissible method for the synthesis of small radiolabeled $BaSO_4$ NPs as carriers for radium combined with a further surface functionalization using alendronate to connect biological targeting moieties.

Results and discussion

Our focus regards the development of a carrier for radium based on alendronate-functionalized $BaSO_4$ NPs, which is prepared in a convenient one-pot reaction in aqueous reaction medium. The co-precipitation is a facile method for this purpose and delivers radium-doped NPs small in size. Additionally, the connection of target-selective (bio)molecules is possible.

Synthesis of alendronate-functionalized $BaSO_4$ NPs

For this purpose, three different systems were investigated for the synthesis of the alendronate-containing NPs: A) cyclohexane/water emulsion systems, B) the reaction in water/THF mixtures and C) simple precipitation in aqueous medium using different reactants and surfactants each. Our aim for the syntheses experiments was to find a simple preparation method for small $BaSO_4$ NPs since it also has to be suitable for future radiolabeling methods.

Syntheses using emulsion reactions

Different methods for microemulsion systems were previously described in the literature, showing a suitable NP-size, but without a functionalization.[40-43] To be able to introduce further molecules on the NP surface, alendronate was chosen as potential surfactant. Thus, 5 mL of a stock solution (containing the barium salt and the respecting surfactant) was reacted with different volumes (2 or 5 mL, see Table 1) of a feeding solution (containing the sulfate salt and surfactants) under a constant flow via a syringe pump at room temperature (rt). The NPs were centrifuged for 30 min at 4500 rpm and redispersed in distilled water. The cycle was repeated three times. The compositions of the starting solutions used in the approaches, the special reaction conditions and solvents as well as the results regarding the average hydrodynamic diameters D_h and polydispersity indices (PDI) are shown in the following Table 1.

Smallest NPs were achieved for experiments **S2** and **S8** with a mean diameter of 132 nm. Co-surfactants like Triton-X100 and n-hexanol did not have any effect on the particle size or size distribution as well as changing the sulfate salt (**S1**-**S4** vs. **S5**-**S8**). Using ultrasound instead of standard stirring conditions with a magnetic stirrer (**S5** vs. **S7**) did not have any influence. To conclude, the emulsion system is hard to influence by the components themselves ($(NH_4)_2SO_4$ vs. Na_2SO_4) or by the used ion concentrations (volumes) and the surfactants, respectively.

Table 1: Preparation conditions and results like the average particle diameter D_h and the polydispersity index (PDI) for the NP synthesis approaches **S1-S8.**

	Stock Solution (5 mL H_2O)	Feeding Solution	Conditions	D_h (nm)	PDI
S1	13 mg $Ba(NO_3)_2$ in cyclohexane	6.6 mg $(NH_4)_2SO_4$ 35 mg alendronate in H_2O/EtOH 50/50 (2 mL)	1000 rpm, rt, 8 mL/h	158	0.169
S2	13 mg $Ba(NO_3)_2$ in cyclohexane	6.6 mg $(NH_4)_2SO_4$ 35 mg alendronate in H_2O (2 mL)	1000 rpm, rt, 8 mL/h	132	0.190
S3	13 mg $Ba(NO_3)_2$ 1.5 g Triton in cyclohexane	6.6 mg $(NH_4)_2SO_4$ 35 mg alendronate in H_2O/EtOH 50/50 (2 mL)	1000 rpm, rt, 8 mL/h	148	0.199
S4	13 mg $Ba(NO_3)_2$ 1.5 g Triton in cyclohexane	6.6 mg $(NH_4)_2SO_4$ 35 mg alendronate in H_2O (2 mL)	1000 rpm, rt, 8 mL/h	238	0.221
S5	13 mg $Ba(NO_3)_2$ in cyclohexane	7.1 mg Na_2SO_4 35 mg alendronate in H_2O (5 mL)	ultrasound, rt, 20 mL/h	218	0.147
S6	13 mg $Ba(NO_3)_2$ 1 g hexanol in cyclohexane	7.1 mg Na_2SO_4 35 mg alendronate in H_2O (5 mL)	ultrasound, rt, 20 mL/h	217	0.131
S7	13 mg $Ba(NO_3)_2$ 410 mg Triton in cyclohexane	7.1 mg Na_2SO_4 35 mg alendronate in H_2O (5 mL)	1000 rpm, rt, 20 mL/h	407	0.423
S8	13 mg $Ba(NO_3)_2$ in cyclohexane	7.1 mg Na_2SO_4 35 mg alendronate in H_2O (5 mL)	1000 rpm, rt, 20 mL/h	132	0.129

Syntheses using water/THF solvent mixtures

The second investigated synthesis method was based on the usage of water/THF solvent mixtures as reaction medium for $BaSO_4$ precipitation.[44] Thus, 5 mL of a feeding solution containing Na_2SO_4 were added via a syringe pump to 5 mL of a stock solution containing $Ba(NO_3)_2$ in THF/water mixtures of different ratios. The NPs were purified as described above. The results of the different approaches as well as all reaction conditions are pointed out in Table 2.

Table 2: Preparation conditions and results like the average particle diameter D_h and the polydispersity index (PDI) for the NP synthesis approaches **S9-S14.**

	Stock Solution (5 mL)	Feeding Solution (5 mL)	Conditions	D_h (nm)	PDI
S9	65 mg $Ba(NO_3)_2$ in H_2O/THF 1/53	7.1 mg Na_2SO_4 in H_2O	1000 rpm, rt, 8 mL/h	229	0.202
S10	65 mg $Ba(NO_3)_2$ in H_2O/THF 1/3.5	7.1 mg Na_2SO_4 in H_2O	1000 rpm, rt, 8 mL/h	5912	0.301
S11	13 mg $Ba(NO_3)_2$ in H_2O/THF 1/53	7.1 mg Na_2SO_4 in H_2O	1000 rpm, rt, 8 mL/h	185	0.181
S12	13 mg $Ba(NO_3)_2$ in H_2O/THF 1/3.5	7.1 mg Na_2SO_4 in H_2O	1000 rpm, rt, 8 mL/h	465	0.399
S13	13 mg $Ba(NO_3)_2$ in THF	7.1 mg Na_2SO_4 in H_2O	1000 rpm, rt, 8 mL/h	146	0.180
S14	13 mg $Ba(NO_3)_2$ 40 mg alendronate in THF	7.1 mg Na_2SO_4 in H_2O	1000 rpm, rt, 8 mL/h	4562	0.459

By comparing the results of the water/THF reaction systems with the results of the microemulsion methods, no further influence of e.g. the organic solvent concerning the reduction of the particle size was detected by DLS. The smallest particles without alendronate (146 nm) were obtained while using the stock solution in 100% THF and the feeding solution in 100% water (**S13**). Surprisingly, the same one-pot procedure with alendronate led to an extreme enhancement of the particle size to the micrometer range (**S14**).

Syntheses using ethanol/water solvent mixtures

Since the reaction systems with cyclohexane/water microemulsion and THF/water did not show any notable advantages, a third method, the precipitation in ethanol/water (v/v = 1/11) was tested. For this purpose, the feeding solution containing different amounts of sulfate was added to the stock solution, containing a fixed amount of Ba^{2+} and alendronate, via a syringe pump using different volume flow rates at different temperatures. All comparable approaches and results regarding the particle size and PDI are demonstrated in Table 3.

According to approach **S15**, the most convenient method delivering the smallest NP size consists of the addition of feeding solution to the stock solution under stirring at 1000 rpm and with a final Ba^{2+}/SO_4^{2-} ratio of 6/1. The precipitation leads to NPs in a diameter of 140 ± 50 nm particle size obtained by DLS (Figure 1). This is in the same range compared to the NPs obtained from the microemulsion method. Based on this result and due to its simplicity, preparation procedure **S15** was used as basis for all following experiments.

To estimate the in vivo behavior and the coagulation properties of the NPs, the zeta potential was measured. It ranged from 15-18 mV, which is acceptable for an in vivo application, but it could risk the interaction with anionic charged biomacromolecules of the body (proteins, cell membranes, etc.).

To verify the precipitation behavior of barium alendronate, one experiment was accomplished with Ba^{2+} in the presence of alendronate without sulfate, which shows no precipitation of barium alendronate itself in water.

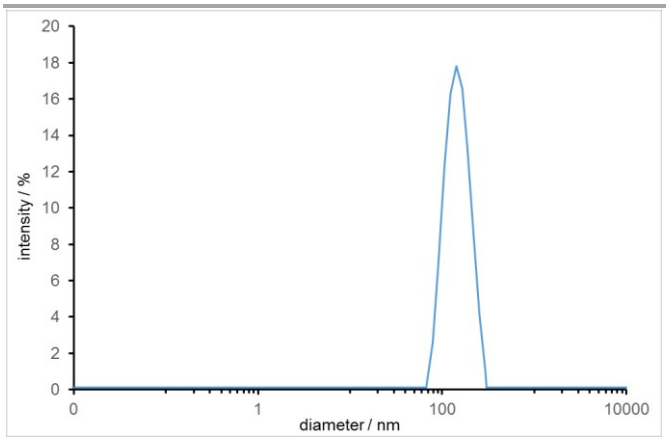

Figure 1. Size distribution of NPs synthesized according to approach **S15** (intensity vs. size) recorded by DLS measurements.

Table 3: Preparation conditions and results like the average particle diameter D_h and the polydispersity index (PDI) for the NP synthesis approaches **S15-S24.**

	Stock Solution (5 mL H_2O)	Feeding Solution (1 mL H_2O/EtOH)	Conditions	D_h (nm)	PDI
S15	61 mg $BaCl_2$ 46 mg alendronate	6.6 mg $(NH_4)_2SO_4$	1000 rpm, rt, 3 mL/h	140	0.076
S16	61 mg $BaCl_2$ 46 mg alendronate	6.6 mg $(NH_4)_2SO_4$	1000 rpm, rt, 2 mL/h	153	0.080
S17	61 mg $BaCl_2$ 46 mg alendronate	6.6 mg $(NH_4)_2SO_4$	1000 rpm, rt, 1 mL/h	158	0.097
S18	61 mg $BaCl_2$ 46 mg alendronate	6.6 mg $(NH_4)_2SO_4$	1000 rpm, 0°C, 3 mL/h	142	0.097
S19	61 mg $BaCl_2$ 46 mg alendronate	6.6 mg $(NH_4)_2SO_4$	1000 rpm, 40°C, 3 mL/h	180	0.117
S20	61 mg $BaCl_2$ 46 mg alendronate	6.6 mg $(NH_4)_2SO_4$	1000 rpm, 80°C, 3 mL/h	174	0.125
S21	61 mg $BaCl_2$ 46 mg alendronate	0.33 mg $(NH_4)_2SO_4$	1000 rpm, rt, 3 mL/h	223	0.147
S22	61 mg $BaCl_2$ 46 mg alendronate	3.3 mg $(NH_4)_2SO_4$	1000 rpm, rt, 3 mL/h	155	0.053
S23	61 mg $BaCl_2$ 46 mg alendronate	33 mg $(NH_4)_2SO_4$	1000 rpm, rt, 3 mL/h	322	0.400
S24	61 mg $BaCl_2$ 46 mg alendronate	6.6 mg $(NH_4)_2SO_4$	utrasound, rt, 3 mL/h	205	0.284

Labeling of the functionalized $BaSO_4$ NPs

The amine groups on the surface of the alendronate-NPs allow a further functionalization with targeting molecules and an introduction of fluorescence labels for dual labeling. Additionally, the one-pot radiolabeling procedures using ^{133}Ba and ^{224}Ra were investigated.

Fluorescence labeling of alendronate NPs

To further investigate the incorporation of the alendronate with the $BaSO_4$, NBD-alendronate **7** containing the 7-nitrobenzo-2-oxa-1,3-diazolyl (NBD) moiety was synthesized according to Scheme 1.

In the first reaction step, the fluorescence dye NBD-chloride **1** was attached to 6-aminohexanoic acid (**2**) for chain length enhancement to give **3** (70% yield). Compound **3** was then reacted with tetrafluorophenol (**4**) to synthesize the TFP-active ester **5** in 78% yield. Finally, active ester **5** was reacted with alendronate (**6**) to connect the NBD-dye motif to the amine site of the alendronate. The final product **7** was obtained in 65% yield and used for further NP syntheses.

NBD-alendronate containing NPs were synthesized according to approach **S15** using a mixture of of NBD-alendronate **7** in alendronate. UV/Vis measurements of washing solutions aimed at the determination of the alendronate wash out during the work-up procedure. An absorption maximum was found for compound **7** at 460-490 nm. Three different syntheses with different NBD-alendronate to alendronate ratios (0.1%, 1% and 2%) were compared and the absorptions of the three work-up solutions were recorded at λ_{max} = 486 nm. It was found that, no matter how much of compound **7** was added to the reaction mixture, approximately 50% of the NBD-alendronate **7** is washed away from the resulting alendronate-NPs within the first work-up step. Wash steps 2 and 3 did not lead to any further significant wash out of **7**. The NBD-containing NPs are

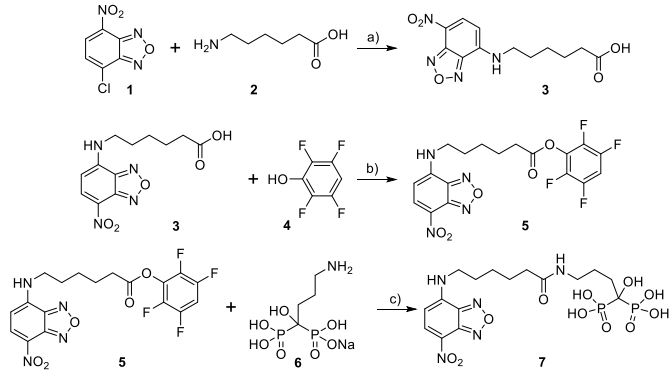

Scheme 1: Synthesis way to NBD-alendronate **7**. Reaction conditions: a) $KHCO_3$, ACN/H_2O 50/50, 65°C, 2 h, inert atmosphere, b) EDC, DCM/ACN, rt, 2 h, c) TEA, DMF, rt, overnight.

saturated with alendronate and are stable against further wash out as well as the unmodified alendronate-NPs.

As the alendronate contains a free amine group, the alendronate-NPs possess amine groups on the surface as well. Consequently, the investigation of the amine reactivity of the alendronate-containing NPs was a matter of particular interest to connect e.g. target molecules for tumor targeting. For this purpose, alendronate-containing $BaSO_4$ NPs without the NBD-dye were synthesized according to approach **S15** and subsequently reacted with an excess of compound **5**. Since compound **5** is an active ester, which reacts readily with amines, the conjugation reaction of **5** with the alendronate-containing NPs was performed under mild conditions (THF/H_2O 1/1, pH 8.5, 2 h, rt) and led to fluorescence-labeled NPs. Afterwards, the particles were centrifuged and washed five times to ensure that most of the starting material **5** was removed from the product. A characterization of the fluorescence-labeled NPs by DLS gave an average particle diameter of 156 ± 56 nm and a zeta potential of +17 mV.

For the fluorescence measurements, all samples were dispersed or dissolved in a THF/H_2O solvent mixture (v/v = 1/1). When the samples were redispersed in pure water, fluorescence was not detectable, likely to solvent interaction effects. Finally, the wash solutions as well as compound **5** and the resulting product were excited at λ = 475 nm, and the emission was recorded from 490-650 nm. All results of the fluorescence spectroscopy measurements are shown in Figure 2.

In Figure 2, a significant shift in the emission maximum of starting compound **5** (red curve, $\lambda_{max} \approx 565$ nm) was observed compared to the final particle solution (green curve, $\lambda_{max} \approx 540$ nm). This is due to the changed bonding conditions for the dye motif. The first wash solution seems to contain a mixture of compound **5** and dye-functionalized NPs, since the absorption maximum was found between both maxima of **5** and the dye-functionalized NPs. The last wash solution shows the same absorption maximum, which is comparable with λ_{max} of the dye-functionalized NPs reasoned by a small particle loss during the work-up procedure. Hence, a reactivity of the alendronate-containing NPs is evidenced and these NPs can be functionalized conveniently with active esters bearing different targeting moieties like glutamate-ureido-based inhibitors of

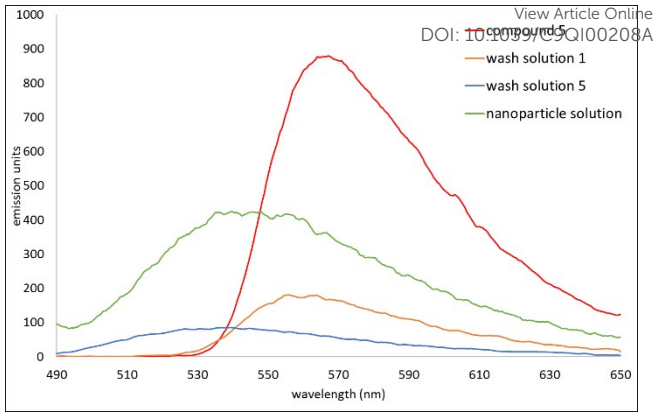

Figure 2. Representative fluorescence spectra for the reaction of alendronate-containing $BaSO_4$ NPs with compound **5** showing the spectra of compound **5** (red), the first (orange) and the last wash solution (blue) of the particle work-up and the final product (green).

prostate-specific membrane antigen (PSMA) or antibodies, which is essential for the progress of our research.

Radiolabeling of alendronate-containing $BaSO_4$ NPs

For future theranostic approaches, the NPs have to be radiolabeled. Thus, the preparation of the radiolabeled $BaSO_4$ NPs was performed according to approach S15 and the addition of the respective radionuclide ^{133}Ba and ^{224}Ra. A 6 to 1 excess of $^{nat}Ba^{2+}$ to SO_4^{2-} was used to determine the amount of the respective radionuclide, which is built into the $BaSO_4$ NP structure.

It was found, that approximately 20% of ^{224}Ra as well as 20% ^{133}Ba were incorporated into the NPs, whereas 80% remained in the supernatant solution.

In order to determine the radiochemical yield, the NP product dispersion was centrifuged after the standard work-up procedure and the count rates of the pellet and the supernatant solutions were measured.

The same centrifugation method was used next for the stability determination of the NPs. Thus, the NP product dispersion was treated with ultrasound and centrifuged at 4500 rpm for 30 min. Activity measurements were performed on the supernatant 1, 2, 3, 4 and 7 days after preparation (Figure 3). Notably, the synthesized alendronate-containing [^{133}Ba]$BaSO_4$ NPs as well as the [^{224}Ra](Ra)$BaSO_4$ NPs showed a very low

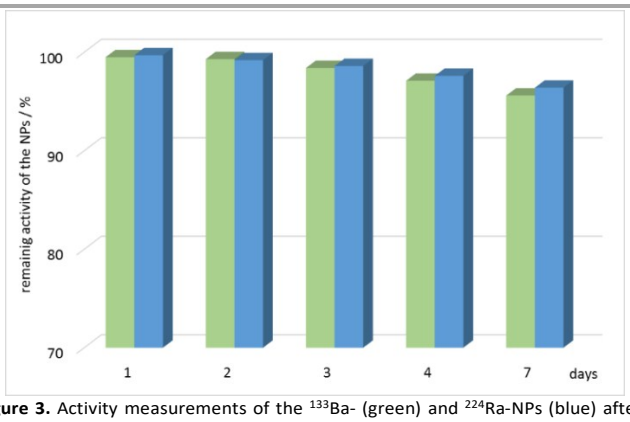

Figure 3. Activity measurements of the ^{133}Ba- (green) and ^{224}Ra-NPs (blue) after treatment with ultrasound and recentrifugation.

activity release of less than 5%, which is sufficient for future therapeutic applications. Avoiding the release of free Ra^{2+} is important, otherwise Ra^{2+} will accumulate into the bones and intestine.[16,17]

Importantly, both radiolabeled NPs showed exactly the same properties compared to the non-radioactive NPs and are stable under aqueous conditions. Thus, we expect, that all results, which were received for the non-radiolabeled NPs, are transferrable to the radiolabeled NPs. Finally, the size distribution of the radium-doped NPs was additionally verified by DLS after 10 half-lives of ^{224}Ra. No significant alteration of the NPs was detected.

Further Characterization of the NPs

Infrared spectroscopy is an excellent tool for the analysis of the NPs due to specific bands resulting from the sulfate and the other functional groups in the particles. Thus, the existence of the alendronate containment was evidenced. Therefore, IR spectra of a) alendronate, b) $BaSO_4$ NPs and c) alendronate-containing $BaSO_4$ NPs (synthesis approach **S15** with and without alendronate) were recorded. The resulting IR spectra are shown in Figure 4.

It is clearly shown in Figure 4b that $BaSO_4$ NPs without any further functionalization are stabilized by a hydrate shell (ν_{OH} = 1410 cm^{-1}, 3100-3400 cm^{-1}). In contrast, alendronate-containing NPs, shown in Figure 4c, do not show this band. Instead, two smaller bands (ν_{NH2} = 1560 cm^{-1}, 1620 cm^{-1}) and the broad primary amine band (ν_{NH2} = 3100-3600 cm^{-1}), belonging to the alendronate motif (see Figure 4a), were determined. From these spectra, it is shown that the $BaSO_4$ NPs without alendronate were initially stabilized by a hydrate shell. When a stabilizing additive like alendronate was added to the reaction mixture, the NP structure is changed. The alendronate is expected to be much more stable due to the bisphosphonate group, which provides anions for the interaction with Ba^{2+} in the particles to create strong complex-like interactions. Those interactions lead to the particle's charge equalization, which would be beneficial for the biodistribution. Additionally, the occurrence of free amine groups on the NP surface was proven by the addition of ninhydrin to the alendronate-containing NPs and the following color reaction.

According to synthesis approach **S15**, four different nanoparticle samples were investigated by TEM imaging, selected-area electron diffraction (SAED), and EDXS analysis in STEM mode. Sample **T1** refers as standard with non-functionalized $BaSO_4$ NPs. Samples **T2** and **T3** are $BaSO_4$ NPs functionalized with alendronate solely and alendronate containing 2% of compound **7**, respectively. **T4** is a sample of alendronate-functionalized NPs that was synthesized alternatively. For this purpose, a sample of **T1** was dispersed in water, an alendronate solution was added for the surface functionalization and the reaction was stirred for 1 hour at room temperature. TEM images of **T1**-**T4** are shown in Figure 5. $BaSO_4$ NPs from **T1** show various shapes and have a smooth surface which agrees with previously published results by a research group focusing on $BaSO_4$ (Figure 5a).[44] Some of them are characterized by a hollow interior. The **T1** particle size was

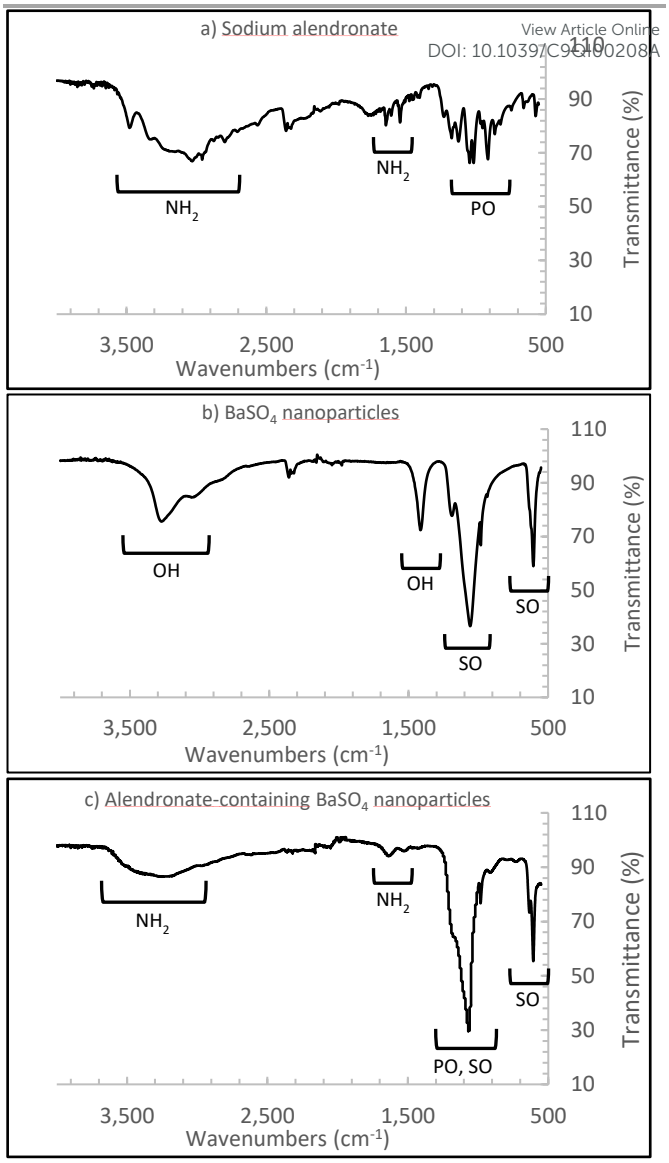

Figure 4. IR spectra (ATR) of a) sodium alendronate (**6**), b) $BaSO_4$ NPs, c) alendronate-containing $BaSO_4$ NPs

determined to 136 ± 57 nm. Alendronate-functionalized $BaSO_4$ particles from **T2** and **T3** are of similar morphology (Figure 5b,c). The particle size was determined to 129 ± 69 nm for **T2** and 124 ± 68 nm for **T3**. Both size distributions are comparable to that of **T1** and on the same order as the particle size analyzed by DLS (140 ± 50 nm). However, compared to **T1**, $BaSO_4$ particles from **T2** and **T3** are of slightly different morphology, showing rough surfaces and no signs of a hollow interior. Such differences between bare and functionalized $BaSO_4$ particles are obviously due to the presence of alendronate during the one-pot synthesis. Functionalizing $BaSO_4$ particles with alendronate in a second step changes the morphology. As shown in Figure 5d, there are **T4** particles with the expected filled-core structure, while some of them show only shell-like behavior. The **T4** particle size was determined to 149 ± 88 nm. SAED analysis of all four samples T1-T4 confirms the orthorhombic barite structure (a = 8.8842(12) Å, b = 5.4559(8) Å, c = 7.1569(9) Å, space group *Pnma* (62)[45]) with small

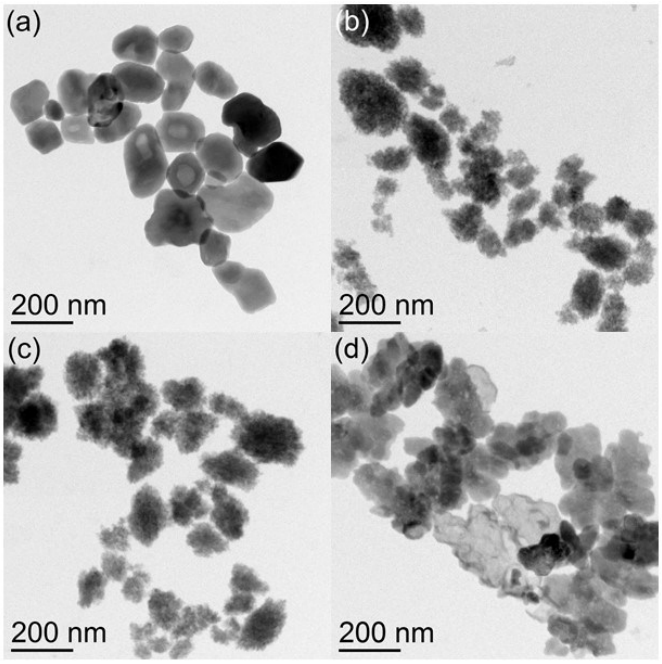

Figure 5: Bright-field TEM images of **T1** (a), **T2** (b), **T3** (c), and **T4** (d).

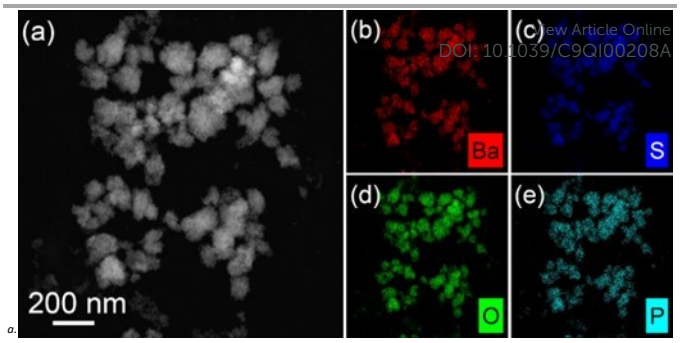

Figure 6: HAADF-STEM image of **T2** (a) together with the corresponding element distributions obtained by EDXS analysis for barium (b), sulfur (c), oxygen (d), and phosphorous (e).

crystallite sizes for T2 and T3 and larger ones for T1 and T4. To qualitatively prove the alendronate functionalization, spectrum imaging analysis based on EDXS was performed for **T2**. While Figure 6a shows a representative HAADF-STEM image for **T2**, the corresponding Ba, S, O and P element distributions are given in Figures 6b-e, respectively. Since the phosphorous signal is homogenously spread across the $BaSO_4$ particles and does not show typical core-shell behavior, the alendronate moiety seems to be distributed over the whole particles and is not only present on the outer NP surface.

Experimental

General

All chemicals were purchased from commercial suppliers and used without further purification. Anhydrous solvents were purchased from Sigma Aldrich. NMR spectra of all synthesized compounds were recorded on Agilent DD2-400 MHz NMR devices with ProbeOne. All chemical shifts of ^{1}H, ^{13}C, ^{19}F and ^{31}P were reported in parts per million using TMS as internal standard for ^{1}H and ^{13}C, $CFCl_3$ for ^{19}F and 85% H_3PO_4 for ^{31}P at 25 °C. All $^{1}H/^{13}C$ spectra were calibrated using the respective solvent signal. Mass spectrometric data were recorded on an Advion Expression CMS using electrospray ionization. Chromatographic analyses and separations were carried out on Merck Silica Gel 60 F_{254} TLC plates and Merck Silica Gel 60, respectively. Automated column flash chromatography was performed on Isolera Four (Biotage) using RP-18 cartridges (SNAP Ultra, C18, 10 g). Dynamic light scattering for the determination of the particle size, the particle size distribution and the zeta potential measurement was performed on a Zetasizer Nano ZS (Malvern Panalytical) using disposable plastic cuvettes. UV/Vis measurements were performed on a Specord 50 (Analytik Jena) instrument and fluorescence measurements on LS 55 by Perkin Elmer. Infrared spectra (ATR) were recorded with a Thermo Fisher Nicolet iS5. $[^{133}Ba]BaCl_2$ was purchased from Polatom. The specific activity A_S from the manufacturers certificate is 50 MBq/mg Ba. $[^{224}Ra]Ra(NO_3)_2$ was separated from a ^{228}Th-source by ion exchange chromatography and was obtained as non carrier added solution. Stock solutions for both radionuclides were adjusted to 1 MBq/mL. Radioactivity count rates were measured using the ISOMED 2160 (MED) sodium iodide detector. Bright-field transmission electron microscopy (TEM) imaging was performed with an image C_s-corrected Titan 80-300 microscope (FEI) operated at an accelerating voltage of 300 kV. To determine their size, 100 particles were analyzed for each sample. The respective particle sizes are given with their standard deviation. To analyze the crystal structure of the synthesized particles, selected-area electron diffraction (SAED) was performed. High-angle annular dark-field scanning transmission electron microscopy (HAADF-STEM) imaging and spectrum imaging analysis based on energy-dispersive X-ray spectroscopy (EDXS) were done at 200 kV with a Talos F200X microscope equipped with a Super-X EDXS detector system (FEI). Prior to TEM analysis, the specimen mounted in a high-visibility low-background holder was placed for 2 s into a Model 1020 Plasma Cleaner (Fischione) to remove possible contaminations. TEM specimens were prepared by dispersing the particles in deionized water, followed by ultrasonication, dropping the particle solution onto carbon-coated copper grids and final drying at ambient temperature.

Procedure for the synthesis of alendronate-containing $BaSO_4$ NPs (approach S15)

A stock solution of 61 mg $BaCl_2$ and 46 mg sodium alendronate (containing 0%, 0.1%, 1% and 2% of compound **7**, respectively) in 5 mL water was prepared. A feeding solution of 6.6 mg $(NH_4)_2SO_4$ in 1 mL ethanol/water (v/v = 1/1) was added via a syringe pump (PHD 2000, Harvard Apparatus) under a constant volume flow rate of 3 mL/h. The reaction was stirred with a magnetic stirrer at 1000 rpm at rt. After the feeding solution was completely added, the solution was allowed to stir for 10 min. The resulting NPs were centrifuged at 4500 rpm for 30 min and redispersed in distilled water. The work-up cycle

View Article Online
DOI: 10.1039/C9QI00208A

was repeated three times and the final product was redispersed in distilled water.

Surface modification of alendronate-containing $BaSO_4$ NPs

Alendronate-containing $BaSO_4$ NPs (synthesized according to approach **S15**, 15 mg) were redispersed in THF/water (50/50). The pH was adjusted to 8 with a Na_2CO_3 solution. 3 mL of compound **5** in THF/water (50/50; pH 8 by Na_2CO_3 adjustment) were added via a syringe pump (3 mL/h) and the reaction was allowed to stir at rt for 3 h. The resulting particles were centrifuged at 4500 rpm for 30 min and the excess of starting material 5 was washed out five times.

Synthesis of radiolabeled [^{133}Ba]$BaSO_4$ and [^{224}Ra](Ra)$BaSO_4$ NPs

A stock solution of 61 mg $BaCl_2$, 50 kBq of [^{133}Ba]$BaCl_2$ or [^{224}Ra]$Ra(NO_3)_2$ and 46 mg sodium alendronate in 5 mL water was prepared. A feeding solution of 6.6 mg $NH_4(SO_4)$ in 1 mL ethanol/water (1/1) was added via a syringe pump (55-1111, Harvard Apparatus) under a constant volume flow rate of 3 ml/h. The reaction was stirred with a magnetic stirrer at 1000 rpm at rt. After the feeding solution was completely added, the solution was allowed to stir for 10 min. The resulting particles were centrifuged at 4500 rpm for 30 min and redispersed in distilled water. The work-up cycle was repeated three times and the final product was redispersed in distilled water.

Organic syntheses

6-((7-Nitro-benz-2-oxa-1,3-diazol-4-yl)amino)hexanoic acid 3

6-Aminohexanoic acid (**2**, 157 mg, 1.2 mmol) and potassium hydrogencarbonate (300 mg, 3 mmol) were dissolved in water (10 mL). 4-Chloro-7-nitro-benz-2-oxa-1,3-diazole (NBD-chloride **1**, 200 mg, 1 mmol) was dissolved in acetonitrile (10 mL) and added under an argon atmosphere. The solution was stirred at 65 °C for 2 h. After reaction control via TLC, the solvents were removed. The residue was redissolved in dichloromethane (20 mL) and the organic phase was washed with a hydrogen carbonate solution (3 x 15 mL). The organic layer was dried over Na_2SO_4, the solvent was removed and the crude product was purified via flash column chromatography (dichloromethane/ methanol 95/5) to yield **3** as an orange solid (205 mg, 70%). R_f=0.16 (CH_2Cl_2/MeOH 95:5); ^{1}H NMR (400 MHz, acetonitrile-d_3, 25°C): δ = 1.41-1.49 (m, 2H, CH_2), 1.58-1.67 (m, 2H, CH_2), 1.71-1.79 (m, 2H, CH_2), 2.29 (t, ^3J = 7.5 Hz, 2H, CH_2CO), 3.51 (br s, 2H, NCH_2), 6.30 (d, ^3J = 8.8 Hz, 1H, ArH), 7.38 (br s, 1H, NH), 8.49 (d, ^3J = 8.8 Hz, 1H, ArH), 8.84 ppm (s, 1H, OH); ^{13}C NMR (101 MHz, acetonitrile-d_3, 25°C): δ = 25.2, 27.0, 28.5 (3xCH_2), 34.1 ($CO\underline{C}H_2$), 44.4 (NCH_2), 99.8, 138.4 (2 x CH_{Ar}), 145.5, 145.8, 146.0, 146.1 (4 x C_{Ar}), 176.7 ppm (C=O); MS (ESI–): *m/z* (%): 293 (100) [M-H]$^-$. elemental analysis calcd (%) for $C_{12}H_{14}N_4O_5$: C 48.98, H 4.80, N 19.04; found: C 49.12, H 4.85, N 19.16.

2,3,5,6-Tetrafluorophenyl 6-((7-nitro-1,2,3-benzoxadiazol-4-yl) amino)hexanoate 5

6-((7-Nitrobenz-2-oxa-1,3-diazol-4-yl)amino)hexanoic acid (**3**, 170 mg, 0.57 mg) and EDC·HCl (125 mg, 0.65 mmol) were dissolved in anhydrous acetonitrile (15 mL). 2,3,5,6-Tetrafluorophenol (**4**, 108 mg, 0.65 mmol) was dissolved in anhydrous dichloromethane (15 mL) and added to **3** under an argon atmosphere. The reaction mixture was stirred for 2 h at rt. After reaction control via TLC, the solvents were evaporated and the residue was redissolved in dichloromethane (20 mL). The organic layer was washed three times (2 x 20 mL saturated hydrogen carbonate, 1 x 20 mL brine) and dried over Na_2SO_4 afterwards. The solvent was removed and the crude product was purified by flash column chromatography (dichloromethane) to yield product **5** as orange solid (205 mg, 78%). R_f=0.39 (CH_2Cl_2); ^{1}H NMR (400 MHz, $CDCl_3$, 25°C): δ = 1.58-1.70 (m, 2H, CH_2), 1.83-1.96 (m, 4H, CH_2), 2.74 (t, ^3J = 7.1 Hz, 2H, CH_2CO), 3.51-3.59 (m, 2H, NCH_2), 6.19 (d, ^3J = 8.6 Hz, 1H, ArH), 6.34 (br s, 1H, NH), 6.94-7.06 (m, 1H, ArH), 8.48 ppm (d, ^3J = 8.6 Hz, 1H, ArH); ^{13}C NMR (101 MHz, $CDCl_3$, 25°C): δ = 24.4, 26.2, 29.3 (3xCH_2), 33.2 ($CO\underline{C}H_2$), 43.7 (NCH_2), 98.7 (CH_{Ar}), 103.4 ($\underline{C}H_{Ar}$), 124.2 (C_{Ar}), 129.7 (C-O), 136.6 (CH_{Ar}), 140.7 (CF_{Ar}), 143.9, 144.0, 144.4 (3xC_{Ar}), 146.2 (CF_{Ar}), 147.4 (CF_{Ar}), 169.3 ppm (C=O); ^{19}F NMR (376 MHz, $CDCl_3$): δ = -153.2 (m, 2F, F_{Ar}), -138.9 ppm (m, 2F, F_{Ar}); MS (ESI–): *m/z* (%): 441 (100) [M-H]$^-$; elemental analysis calcd (%) for $C_{18}H_{14}F_4N_4O_5$: C 48.88, H 3.19, N 12.67; found: C 48.81, H 3.26, N 12.58.

(1-Hydroxy-4-(6-((7-nitrobenz-2-oxa-1,3-diazol-4-yl)amino)hexanamido)butane-1,1-diyl)bis(phosphonic acid) 7

2,3,5,6-Tetrafluorophenyl 6-((7-nitrobenz-2-oxa-1,3-diazol-4-yl)amino)hexanoate (**5**, 100 mg, 0.22 mmol), sodium alendronate trihydrate (**6**, 71 mg, 0.22 mmol) and Et_3N were dissolved in DMF/H_2O (50/50, 20 mL). The reaction mixture was allowed to stir at rt overnight. After reaction control via TLC, the solvents were removed and the residue was redissolved in ethyl acetate (20 mL). The organic layer was washed with hydrogen sulfate (3 x 20 mL) and dried over Na_2SO_4. The crude product was purified by automated reverse phase flash column chromatography (water, 0.5% TFA) to yield **7** as orange-red solid (97 mg, 69%). R_f=0.58 (RP, ACN/H_2O 50/50, 0.1% TFA); ^{1}H NMR (400 MHz, D_2O, 25°C): δ = 1.41-1.51 (m, 2H, CH_2), 1.62-1.72 (m, 2H, CH_2), 1.76-1.87 (m, 4H, CH_2), 1.98-2.10 (m, 2H, CH_2), 2.29 (t, ^3J = 7.3 Hz, 2H, CH_2), 3.17-3.25 (m, 2H, CH_2), 3.57-3.68 (m, 2H, CH_2), 6.43 (d, ^3J = 9.1 Hz, 1H, Ar-H), 8.54 ppm (d, ^3J = 9.1 Hz, 1H, Ar-H); ^{13}C NMR (101 MHz, D_2O, 25°C): δ = 23.2, 24.9, 25.6, 27.1, 30.8, 34.4, 35.6, 39.6 (CH_2), 43.5 (C-P), 100.1 (CH_{Ar}), 119.7, 126.7 (2xC_{Ar}), 128.6 (CH_{Ar}), 139.2 (C_{Ar}), 144.3 (C_{Ar}), 176.8 ppm (C=O); ^{31}P NMR (243 MHz, D_2O, 25°C): δ = 19.4 ppm; MS (ESI+): *m/z* (%): 526 (72) [M+H]$^+$, 548 (100) [M+Na]$^+$; elemental analysis calcd (%) for $C_{16}H_{24}N_5NaO_{11}P_2$: C 35.11, H 4.42, N 12.80; found: C 34.99, H 4.40, N 12.66.

Conclusions

A novel strategy for the modification of radiolabeled NPs for TAT was developed. For this purpose, a facile procedure for the synthesis of functionalized $BaSO_4$ NPs and their radiolabeled ^{224}Ra and ^{133}Ba analogs was established. By comparing different reaction parameters, a simple preparation in ethanol/water

was found to be the most suitable, delivering the smallest NPs in diameter under the applied conditions. Particle size distributions were determined by dynamic light scattering (DLS) and verified by transmission electron microscopy (TEM), respectively. The functionalization of $BaSO_4$ NPs was successfully accomplished with alendronate as additive in a one-pot reaction. The existence of the particle modification was verified by infrared spectroscopy and by the substitution of alendronate by NBD-alendronate-containing alendronate, followed by UV/Vis- and fluorescence spectroscopy, respectively. Furthermore, an additional surface modification regarding targeting purposes was examined by reacting the alendronate-containing $BaSO_4$ NPs with the TFP-active ester **5**. The control of the reaction success was performed by fluorescence spectroscopy. In consequence, alendronate-containing $BaSO_4$ NPs were synthesized and their further reactivity was successfully assured by active ester coupling. To obtain smaller particles for future works, it may be helpful to investigate further methods using more complex equipment for nanomilling or operating in a spinning-disc reactor. Moreover, several literature-known size control methods for NP synthesis can be investigated. Our future research, after reaching smaller particle sizes and sharper distributions, will concentrate on attaching several biological targeting units, like glutamate-ureido-based inhibitors of PSMA or antibodies, to the alendronate-containing $[^{131}Ba/^{224}Ra](Ra)BaSO_4$ NPs and preparing initial biological studies.

Conflicts of interest

There are no conflicts to declare.

Notes and references

1 B. Allen, *J. Biomed. Phys. Eng.*, 2013, **3**, 67.
2 B. J. Allen, C. Y. Huang, R. A. Clarke, *Biol. Targets Ther.*, 2014, **8**, 255.
3 M. Gott, J. Steinbach, C. Mamat, *Open Chem*., 2016, **14**, 118.
4 C. Kratochwil, F. Bruchertseifer, F. L. Giesel, M. Weis, F. A. Verburg, F. Mottaghy, K. Kopka, C. Apostolidis, U. Haberkorn, A. Morgenstern, *J. Nucl. Med.*, 2016, **57**, 1941.
5 T. Nayak, J. Norenberg, T. Anderson, R. Atcher, *Cancer Biother. Radiopharm.*, 2005, **20**, 52.
6 F. Graf, J. Fahrer, S. Maus, A. Morgenstern, F. Bruchertseifer, S. Venkatachalam, C. Fottner, M. M. Weber, J. Huelsenbeck, M. Schreckenberger, B. Kaina, M. Miederer, *PLoS One*, 2014, **9**, e88239.
7 T. I. Kostelnik, C. Orvig, *Chem. Rev.*, 2019, **119**, 902.
8 B. Mo Kim, Y. Hong, S. Lee, P. Liu, J. H. Lim, Y. H. Lee, T. H. Lee, K. T. Chang, Y. Hong, *Int. J. Mol. Sci*., 2015, **16**, 26880.
9 O. Bruland, T. Jonasdottir, D. Fisher, R. Larsen, *Curr. Radiopharm.*, 2008, **1**, 203.
10 G. Vaidyanathan, M. R. Zalutsky, *Curr. Radiopharm.*, 2011, **4**, 283.
11 H. Jadvar, D. I. Quinn, *Clin. Nucl. Med.*, 2013, **38**, 966.
12 A. S. Abi-Ghanem, M. A. McGrath, H. A. Jacene, *Semin. Nucl. Med.*, 2015, **45**, 66.
13 N. D. Shore, *Urology*, 2015, **85**, 717.
14 K. Yong, M. W. Brechbiel, *Dalton Trans.*, 2011, **40**, 6068.
15 K. Yong, M. Brechbiel, *AIMS Med. Sci.*, 2015, **2**, 228.
16 J. Kozempel, O. Mokhodoeva, M. Vlk, *Molecules*, 2018, **23**, 1.
17 R. M. de Kruijff, H. T. Wolterbeek, A. G. Denkova, *Pharmaceuticals*, 2015, **8**, 321.
18 K. Washiyama, R. Amano, J. Sasaki, S. Kinuya, N. Tonami, Y. Shiokawa, T. Mitsugashira, *Nucl. Med. Biol.*, 2004, **31**, 901.
19 D. Bauer, M. Gott, J. Steinbach, C. Mamat, *Spectrochim. Acta A*, 2018, **199**, 50.
20 J. Steinberg, D. Bauer, F. Reissig, M. Köckerling, H. J. Pietzsch, C. Mamat, *ChemOpen*, 2018, **7**, 432.
21 X. Y. Chen, M. Ji, D. R. Fisher, C. M. Wai, *Inorg. Chem.*, 1999, **38**, 5449.
22 J. Kozempel, M. Vlk, E. Málková, A. Bajzíková, J. Bárta, R. Santos-Oliveira, A. Malta Rossi, *J. Radioanal. Nucl. Chem.*, 2014, **304**, 443.
23 G. Henriksen, B. W. Schoultz, T. E. Michaelsen, O. S. Bruland, R. H. Larsen, *Nucl. Med. Biol.*, 2004, **31**, 441.
24 H. A. Doerner, W. M. Hoskins, *J. Am. Chem. Soc.*, 1925, **47**, 662.
25 M. Grive, F. Grandia, J. Merino, L. Duro, J. Bruno, *Geochim. Cosmochim. Acta*, 2007, **71**, 356.
26 J. Kozempel, M. Vlk, M. Floriánová, B. Drtinová, M. Němec, *J. Radioanal. Nucl. Chem.*, 2014, **304**, 337.
27 M. J. Meagher, B. Leone, T. L. Turnbull, R. D. Ross, Z. Y. Zhang, R. K. Roeder, *J. Nanopart. Res.*, 2013, **15**, 2146.
28 C. Fang, R. Hou, K. Zhou, F. Hua, Y. Cong, J. Zhang, J. Fu, Y.-J. Cheng, *J. Mater. Chem. B*, 2014, **2**, 1264.
29 D. Schwotzer, H. Ernst, D. Schaudien, H. Kock, G. Pohlmann, C. Dasenbrock, O. Creutzenberg, *Part. Fibre Toxicol.*, 2017, **14**, 23.
30 R. Landsiedel, L. Ma-Hock, K. Wiench, W. Wohlleben, U. G. Sauer, *J. Nanopart. Res.*, 2017, **19**, 171.
31 D. Newton, A. K. Ancill, K. E. Naylor, R. Eastell, *Radiat. Prot. Dosim.*, 2001, **97**, 231.
32 M. F. McLaughlin, J. Woodward, R. A. Boll, J. S. Wall, A. J. Rondinone, S. J. Kennel, S. Mirzadeh, J. D. Robertson, *PLoS One*, 2013, **8**, e54531.
33 A. Piotrowska, E. Leszczuk, F. Bruchertseifer, A. Morgenstern, A. Bilewicz, *J. Nanopart. Res.*, 2013, **15**, 2082.
34 J. V. Rojas, J. D. Woodward, N. Chen, A. J. Rondinone, C. H. Castano, S. Mirzadeh, *Nucl. Med. Biol.*, 2015, **42**, 614.
35 A. Piotrowska, S. Meczynska-Wielgosz, A. Majkowska-Pilip, P. Kozminski, G. Wojciuk, E. Cedrowska, F. Bruchertseifer, A. Morgenstern, M. Kruszewski, A. Bilewicz, *Nucl. Med. Biol.*, 2017, **47**, 10.
36 E. L. Zimmerman, E. B. Dale, D. G. Thomas, J. D. Kurbatov, *Phys. Rev.*, 1950, **80**, 908.
37 R. P. Spencer, R. C. Lange, S. Treves, *J. Nucl. Med.*, 1971, **12**, 216.
38 R. P. Spencer, R. C. Lange, S. Treves, *J. Nucl. Med.*, 1970, **11**, 95.
39 N. I. Ivanova, D. S. Rudelev, B. D. Summ, A. A. Chalykh, *Colloid J.*, 2001, **63**, 714.
40 J. Shi, H. Verweij, *Langmuir*, 2005, **21**, 5570.
41 M. Moosa, M. Ikram, S. Ali, Islah-U-Din, J. Optoelectron. *Adv. Mater.*, 2016, **18**, 847.
42 B. Niemann, P. Veit, K. Sundmacher, *Langmuir*, 2008, **24**, 4320.
43 L. I. Boguslavskii, T. M. Buslaeva, V. V. Fomichev, E. V. Kopylova, A. P. Kaplun, V. I. Popenko, *Russ. J. Phys. Chem. A*, 2014, **89**, 256.
44 Á. B. Sifontes, E. Cañizales, J. Toro-Mendoza, E. Ávila, P. Hernández, B. A. Delgado, G. B. Gutiérrez, Yraida Díaz, E. Cruz-Barrios, *J. Nanomat.*, **2015**, 510376.
45 R. J. Hill, *Can. Mineral.*, 1977, **15**, 522.